JOURNAL OF MATERIALS SCIENCE: MATERIALS IN MEDICINE 8 (1997) 365–368

Electrochemical and surface modifications on N^+-ion-implanted 316L stainless steel

E. LEITÃO[1,2], R. A. SILVA[1,3], M. A. BARBOSA[1]
[1] *INEB – Instituto de Engenharia Biomédica, Praça do Coronel Pacheco, 1, 4050 Porto, Portugal*
[2] *FEUP – Faculdade de Engenharia da Universidade do Porto, Rua dos Bragas, 4099 Porto Codex, Portugal*
[3] *ISEP – Instituto Superior de Engenharia do Porto, Rua de S. Tomé, 4200 Porto, Portugal*

The effect of nitrogen-ion implantation on the electrochemical behaviour of 316L stainless steel in a simulated physiological solution (HBSS-Hank's Balanced Salt Solution) was studied by open-circuit potential versus time and cyclic polarization techniques, with the aim of characterizing the surfaces and choosing the best nitrogen-ion fluence. Three fluences (10^{15}, 10^{16} and 10^{17} ions/cm^2) were used. The 10^{16} ions/cm^2 N^+ fluence improves the corrosion resistance of the 316L stainless steel.

1. Introduction

Metals such as stainless steel, titanium alloys and cobalt/chromium alloys are the materials most widely used as orthopaedic prostheses. Stainless steel has good mechanical properties, but has the lowest corrosion resistance among the most common metallic biomaterials [1–3].

The *in vitro* corrosion of stainless steel in physiological solutions shows that toxic ions such as Cr, Ni and Mo are present both in the solutions and in the corrosion products. Puleo and Huh [4] performed a series of cytotoxicity tests on rat bone marrow stromal cells. The ranking of the ions with respect to their toxicity effects was: $Cr^{6+} > Mo^{6+} \approx Fe^{3+} > Co^{2+} > Ni^{2+}$. The presence of these ions *in vivo* may result in the appearance of local inflammatory reactions and ultimately in the loosening of the implant [5–7].

Studies performed on mice by Pereira *et al.* [8] indicate that metallic ions resulting from the corrosion of stainless steel accumulate in the liver and kidneys and are responsible for morphological changes in these organs. It is not possible to extrapolate this model to the human body but these results may indicate that the extent of the damage provoked by the corrosion of stainless steel implants may not occur immediately after implantation in the human body.

Wear of total joint replacements is responsible for the accumulation of debris around the implant, resulting in the long-term failure of these prostheses. The mechanism of aseptic loosening is not fully understood but it has been found that along with the metal debris, macrophages and T-lymphocytes are present around the implant. This indicates the close relationship between the cells and wear particles. It is therefore probable that improving the wear properties of the joint prostheses will improve their longevity [9, 10].

Ion implantation is a surface-treatment technique that modifies a material's surface characteristics. Microstructural defects due to the interaction between the ions of the ion beam and the atoms of the target are produced in the latter. These defects may be responsible for modifications in wear and corrosion resistance and biocompatibility. High-fluence nitrogen ion implantation improves the tribological properties of titanium alloys [10]. It is known that iron nitride precipitates are formed as a result of the nitrogen-ion-implantation process [11] and their presence is assumed to be responsible for the enhancement in wear resistance found on nitrogen-ion-implanted iron [12].

Howlett *et al.* have studied the influence of several ion-implanted ions on silicon wafers [13] and Mg onto alumina [14]. In the first case, they found no evidence that ion-beam implantation with nitrogen, phosphorus, manganese or magnesium ions produces an increase in adhesion of human bone-derived cells to silicon substrata. Nevertheless, they found an increase in the attachment of cells to surfaces which were ion implanted with oxygen. In the second case, they detected an increase in both attachment and spreading of human bone-derived cells on Mg ion-implanted alumina compared to the non-implanted surfaces. *In vivo* studies performed by Johansson *et al.* [9] on rabbit cortical bone showed no major differences between nitrogen ion-implanted titanium and Ti–6Al–4V and the non-implanted materials after three months insertion. Röstlund *et al.* [15] found no significant differences between nitrogen-ion-implanted and non-implanted titanium after 1 week of implantation into the abdominal wall of rats. It was found that nitrogen-ion-implantation changed the biological properties of pure titanium only six weeks after the surgery.

0957–4530

The effect of several ion-implanted N^+ fluences on the corrosion behaviour of 316 L stainless steel in HBSS has been studied in this work. Electrochemical techniques, namely open-circuit potential versus time and cyclic polarization, were used to determine which fluence would induce the best corrosion performance.

X-ray photo-electron spectroscopy (XPS) studies were also carried out, before and after the electrochemical experiments, in order to determine surface modifications induced by the ion-implantation process.

2. Materials and methods

316 L stainless steel samples (Aubert & Duval), 20 mm in diameter and 3 mm thick, were implanted with three different fluences of N^+ ions, namely: 10^{15}, 10^{16} and 10^{17} ion/cm^2, with a beam energy of 40 keV.

Before the electrochemical experiments the samples were ultrasonically degreased with acetone, thoroughly washed with de-ionized water and dried. The electrical connection was made via a copper electrical wire (diameter 0.5 mm) and by applying colloidal silver at the region of contact. The electrical junction was protected by polytetrafluorethylene tape, followed by the application of a non-conductive and water-resistant varnish (Lacomit®), as described in previous work [16].

The electrochemical cell was made of metilpenthen polymer and had a capacity of 150 ml. All experiments were performed at room temperature ($18 \pm 2\,^{\circ}$C) in Hank's Balanced Salt Solution (Gibco), which was deaerated with argon for at least 15 min before the tests. The electrolyte composition was the following (g/l): 0.185 $CaCl_2$, 0.4 KCl, 0.06 KH_2PO_4, 0.1 $MgCl_2 \cdot 6H_2O$, 0.1 $MgSO_4 \cdot 7H_2O$, 8.00 NaCl, 0.35 $NaHCO_3$, 0.48 Na_2HPO_4 and 1.00 D-glucose. All potentials were measured against the saturated calomel electrode (SCE) and are given on this scale. The counter-electrode was a square platinum sheet of area 800 mm^2.

The electrochemical experiments were performed with an EG&G Princeton Applied Research, model 273 A, potentiostat. The potentials were controlled and the data were recorded with the help of software model M352, from EG&G Princeton Applied Research. Several electrochemical parameters were determined using the least squares method, employing successive iterations of the Stearn–Geary equation. Monitoring of the potential as a function of time was carried out for one hour before initiating the potential sweep. In cyclic polarization measurements the potential sweep rate was 10^{-3} V/s starting 0.25 V below the corrosion potential, E_{corr}. The reverse sweep finished when the downward curve was well defined.

After the corrosion measurements, the samples were washed with de-ionized water and dried in air. The surfaces were observed by scanning electron microscopy (SEM) and analysed by XPS. XPS analysis was performed both on as-implanted samples and after corrosion measurements. A VG Scientific ESCALAB, using MgK_α as source, was used to obtain the spectra.

3. Results and discussion

3.1. Electrochemical studies

Fig. 1 gives curves obtained in the open-circuit measurements. A non-implanted surface was used as reference. The figure shows that ion implantation with 10^{15} ions/cm^2 has no significant influence on the final potential. Fluences of 10^{16} and 10^{17} ions/cm^2 displace the curves towards more noble potentials. A dose of 10^{16} ions/cm^2 produces the highest shift in potential. This may be due to the existence of more noble surface layers, formed during the ion-implantation process.

Fig. 2 shows the cyclic polarization curves. All materials, including the non-implanted stainless steel, show very low corrosion current densities in the range of nA/cm^2. Fig. 3 shows a schematic representation of a polarization curve where some parameters are signalled, namely: the passivation potential, E_{pass}, the passivation current density, i_{pass} and the pitting potential, E_p.

Observing the curves presented in Fig. 2, one notices that the lowest fluence gives a first anodic current density maximum (E_{pass}) at -0.28 V, with a passive step up to 0 V. Between 0 V and 0.5 V, a rise in current was detected which was probably due to localized corrosion. Above this point, transients in current were detected. This indicates the initiation and recovery of pits formed on the surface. Above 0.75 V (E_p) a sharp rise in current was observed as a result of pitting

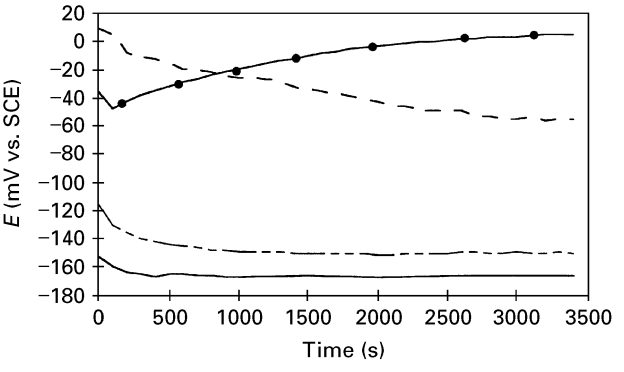

Figure 1 Open-circuit potential versus time curves for 316 L stainless steel not implanted and ion-implanted with three fluences of N^+ at 40 keV: — not-implanted; —--— 10^{15} ions/cm^2; –●– 10^{16} ions/cm^2; ––– 10^{17} ions/cm^2.

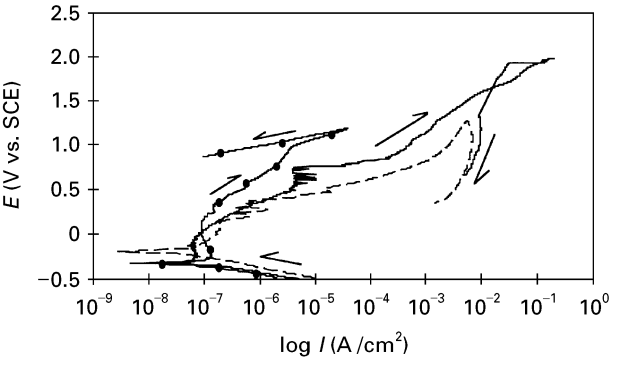

Figure 2 Cyclic polarization curves for 316 L stainless steel ion-implanted with three fluences of N^+ at 40 keV: — 10^{15} ions/cm^2; –●– 10^{16} ions/cm^2; ––– 10^{17} ions/cm^2.

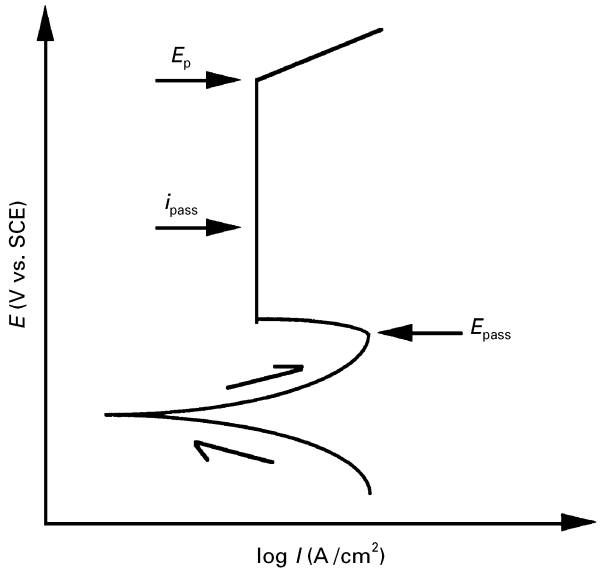

Figure 3 Schematic representation of a polarization curve.

attack. The currents detected on the reverse scan were higher than those on the forward scan, indicating corrosion of the surface. SEM observations, after the electrochemical experiments, showed the presence of pits on the surface. Similar electrochemical behaviour was revealed by the ion-implanted materials with the highest dose. In this case E_{pass} was not evident and the transition potential to the passive state could not be determined. The E_p was lower than in the samples implanted with 10^{15} ions/cm^2. SEM observations of ion-implanted materials with 10^{16} ions/cm^2 showed the presence of no pits. The cyclic polarization curves showed that the recorded currents on the reverse scan were lower than those on the forward scan. The highest potential reached before a sharp rise in current was detected at 0.96 V. This potential was considered as the "pitting potential" to allow a comparison with the other materials. At this potential, the 10^{16} ions/cm^2 sample exhibited the lowest current density of the three ion-implanted samples.

The comparison between the corrosion resistances of these materials can be made by comparing essential potentials in these curves [17], namely the passivation potential and the pitting potential, as schematically shown in Fig. 3.

The protective characteristics of a passive film are shown by the value of i_{pass}. The lower this value the higher are its protective properties. Comparing the values of E_p between these materials gives information on their resistance to localized attack. A material's resistance to localized attack is directly proportional to the value of E_p.

The values, taken from curves similar to those in Fig. 2, are given in Table I. The corrosion potential, E_{corr}, and the passivation current, i_{pass}, are also given and the values obtained are the average of two results.

Analysis of the values given in Table I shows that N^+-ion implantation does not change the corrosion resistance significantly. The E_p were similar on all studied materials except for the highest fluence where a decrease in E_p of around 0.50 V was registered. On

TABLE I Summary of the electrochemical data

Fluence (ions/cm^2)	E_{corr}[a] (V)	E_{pass} (V)	E_p (V)	i_{pass} (A/cm^2)
Non-implanted	− 0.17	–	0.85	2.8×10^{-6}
10^{15}	− 0.15	− 0.29	0.75	4×10^{-6}
10^{16}	− 0.028	− 0.25	0.96	2×10^{-6}
10^{17}	− 0.065	–	0.38	4×10^{-7}

[a] Measured in open-circuit experiments.

the other hand, the highest fluence exhibited the lowest i_{pass}. According to Rauschenbach and Kolitsch [18] implantation of N^+ in Fe results in crystalline phases in the range 1×10^{16} to 1×10^{18} ions/cm^2 · γ-austenite appears in the entire range, but from fluences higher than 4×10^{16} ions/cm^2 other nitride phases appear simultaneously, namely α″-$Fe_{16}N_2$, ε-Fe_2N_{1-x} and α′-martensite [18, 19]. The presence of γ-austenite was also reported by Carbucicchio *et al.* [20] for fluences in the range 5×10^{16} to 1×10^{17} ions/cm^2. Other authors have reported the formation of other nitride phases in steel but all these studies were conducted with ion-implantation doses higher than 2×10^{17} ions/cm^2 [21, 22].

The nature of the precipitates formed during nitrogen-ion implantation varies with the carbon concentration and also with the implanted dose. It seems that the carbon concentration and the dose of nitrogen implantation are two competitive factors, whose combination determines the total amount of iron nitrides that will be formed [22]. Results for stainless steel show that the amount and size of nitrides in the as-implanted material increase with the dose, the proportion of nitrides in stainless steel being almost the same as in pure iron at each dose [12, 18, 22].

The results obtained herein may be explained by the formation of iron nitrides as a consequence of the ion-implantation process. A joint effect between the formation of γ-austenite, α″-$Fe_{16}N_2$, ε-Fe_2N_{1-x} and α′-martensite and an increase in size of the iron nitrides may explain the low E_p exhibited by the 10^{17} ions/cm^2 samples. Larger precipitates will tend to detach from the metallic matrix increasing the area of attack. For the 10^{15} ions/cm^2 the γ-austenite formed may be coherent with the metallic matrix in such a way that no significant changes in the electrochemical parameters have been registered. Ion implantation with 10^{16} ions/cm^2 produces a rise towards more noble potentials of the E_p and a slight reduction of the i_{pass} compared to that of the non-implanted material. Changes in the oxide film composition may explain both these results and the fact that no pits were seen after the cyclic polarization experiments.

3.2. Surface characterization

Survey spectra were acquired before and after corrosion measurements. Following spectra acquisition, peak identification and quantification were achieved using VG Scientific ESCALAB package software. All spectra were calibrated using C1s binding energy, Eb, C1s = 285.0 eV, as reference. All samples exhibited a

TABLE II XPS quantification data for the 316L stainless steel ion implanted with 10^{15}, 10^{16} and 10^{17} ions/cm^2 N^+ at 40 keV

Fluence (ions/cm^2)	Fe (at %)	Cr (at %)	Ni (at %)	N (at %)	O (at %)	Ca (at %)	P (at %)
10^{15}	1.41	3.18	–	2.75	37.19	1.34	1.67
10^{16}	2.67	0.2	0.2	1.6	42.7	3.16	8.62
10^{17}	1.08	3.38	–	0.98	41.3	0.75	3.41

well-defined C1s peak, which is usually a common contaminant.

Table II compares the XPS quantification data for samples which were submitted to corrosion testing. Calcium and phosphorus were detected on all surfaces after corrosion testing but the highest concentrations were found for the 10^{16} ions/cm^2 fluence. On all surfaces a higher concentration of P than Ca was detected.

Electrochemical experiments performed on 316 L stainless steel by Sousa and Barbosa [23] in calcium phosphate and protein solutions showed that there was an inhibition of corrosion caused by the presence of calcium and phosphate ions. It was determined that these ions influence the kinetics of film growth and its thickness. On solutions where Ca and P were present a rise of the E_p was noticed. The increase in thickness is consistent with increased breakdown potentials, since thicker films should require higher electrode potentials The rupture of the passive films depends on a series of factors, namely their composition, structure and thickness. It was also determined that calcium phosphate acts as an inhibitor of pit propagation.

It seems that the material surface structure resulting from nitrogen-ion implantation with 10^{16} ions/cm^2 allows the formation of more protective films whose composition, formed during polarization, is richer in Ca and P. The incorporation of these ions on the film formed during the anodic polarization may explain the high potentials attained without film breakdown. The presence of these ions in the surface film may interfere with the *in vivo* behaviour of the stainless steel implants as it is known that calcium phosphates enhance the bone formation at their surface [24].

4. Conclusions

Nitrogen-ion implantation with 10^{16} ions/cm^2 slightly improves the corrosion resistance of 316 L stainless steel. The formation of more stable films as a consequence of the ion-implantation process may explain this behaviour.

Fluences of 10^{15} ions/cm^2 do not bring any improvement and 10^{17} ions/cm^2 reduces the i_{pass}.

Corrosion of 316 L stainless steel in HBSS produces a calcium- and phosphate-rich surface layer.

Acknowledgements

This work was carried out under project BRITE/EURAM nr. 91-0477. The authors thank Laboratoire PHASE-Strasbourg, France, for providing the ion-implanted samples. Thanks are also due to Dr Carlos Sá for his assistance with the XPS work. E. Leitão was supported by a grant from the Ciencia/Praxis programmes.

References

1. K. H. W. SEAH and X. CHEN, *Corros. Sci.* **34** (1993) 1841–1851.
2. A. C. FRAKER, A. W. RUFF, P. SUNG, A. C. VAN ORDEN and K. M. SPECK, "Titanium alloys in surgical implants", ASTM STP 796, edited by H. A. Luckey and F. Kublei Jr., pp. 206–219 (1983).
3. Y. NAKAYAMA, T. YAMAMURO, P. KUMAR, K. SHIMISU, Y. KOTOURA, M. OKA, J. KWAFUKU and T. TAKASHIMA, *J. Appl. Biomater.* **1** (1990) 307–313.
4. D. A. PULEO and W. W. HUH, *ibid.* **6** (1995) 109–116
5. J.-E. SUNDGREEN, P. BODÖ and I. LUNDSTRÖM, *J. Colloid Interface Sci.* **110** (1986) 9–20.
6. K. MERRIT and S. A. BROWN, *J. Biomedical Mater. Res.* **29** (1995) 627–633.
7. K. MERRIT and S. A. BROWN, *Tech. Orthop.* **8** (1994) 228–236.
8. M. L. PEREIRA, A. M. ABREU, J. P. SOUSA and G. S. CARVALHO, *J. Mater. Sci. Mater. Med.* **6** (1995) 523–527.
9. C. B. JOHANSSON, J. LAUSMAA, T. RÖSTLUND and P. THOMSEN, *ibid.* **4** (1993) 132–141.
10. F. BERNARD, J. DUPUY-PHILON, J. BERT, D. REMY, B. MOYEN and J. L. BESSE, "Advances in materials science and implant orthopaedic surgery", edited by R. Kossowsky and N. Kossowsky, NATO-ASI series E: Applied Science, Vol. **24** (1995) pp. 195–206.
11. B. RAUSCHENBACH, *Nucl. Instrum. Methods Phys. Res.* **B53** (1991) 35–45.
12. B. RAUSCHENBACH, A. KOLITSCH and K. HOHMUTH, *Phys. Status Solidi* (*a*) **80** (1983) 471–482.
13. C. R. HOWLETT, M. D. M. EVANS, K. L. WILDISH, J. C. KELLY, L. R. FISHER, G. W. FRANCIS and D. J. BEST, *Clin. Mater.* **14** (1993) 57–64.
14. C. R. HOWLETT, H. ZREIQAT, R. O'DELL, J. NOORMAN, P. EVANS, B. A. DALTON, C. McFARLAND and J. G. STEELE, *J. Mater. Sci. Mater. Med.* **5** (1994) 715–722.
15. T. RÖSTLUND, P. THOMSON, L. M. BJURSTEN and L. E. ERICSON, *J. Biomed. Mater. Res.* **24** (1990) 847–860.
16. E. LEITÃO, C. SÁ, R. A. SILVA, M. A. BARBOSA and H. ALI, *Corros. Sci.* **37** (1995) 1861–1866.
17. M. A. BARBOSA, *Portugaliae Electrochimica Acta* **7** (1989) 567–590.
18. B. RAUSCHENBACH and A. KOLITSCH, *Phys. Status Solidi* (*a*) **80** (1983) 211–222.
19. B. RAUSCHENBACH, *Nucl. Tracks Radiat. Meas.* **19** (1991) 943–946.
20. M. CARBUCICCHIO, L. BARDANI and S. TOSTO, *J. Appl. Phys.* **52** (1981) 4589.
21. W. W. HU, H. HERMAN, C. R. CLAYTON, J. KOZUBOWSKI, R. A. KANT, J. K. HIRVONEN and R. K. MACCRONE, Surface related mechanical properties of nitrogen implanted 1018 steel. "Proc. ion implantation metallurgy", edited by C. M. Preece and J. K. Hirvonen (AIME, Warrendale, Cambridge, MA, 1979) p. 92.
22. C. A. DOS SANTOS, M. BEHAR, J. P. de SOUZA and I. J. R. BAUMVOL, *Nucl. Instrum. Methods* **209/210** (1983) 907–912.
23. S. SOUSA and M. A. BARBOSA, *J. Mater. Sci. Mater. Med.* **2** (1991) 19–26.
24. C. A. P. T. KLEIN, P. PATKA, J. G. C. WOLKE, J. M. A. de BLIECK-HOGERVORST and K. de GROOT, *Biomaterials* **15** (1994) 146–150.

Received 2 July
and accepted 7 August 1996